# Modeling acoustic backscatter from kidney microstructure using an anisotropic correlation function

Michael F. Insana
*Department of Radiology, University of Kansas Medical Center, 3901 Rainbow Boulevard, Kansas City, Kansas 66160-7234*

(Received 3 May 1994; accepted for publication 15 August 1994)

Techniques for investigating acoustic backscatter from anisotropic biological tissues are examined. This empirical study combines single-scatter theory with the known elastic properties and histology of the renal cortex to predict the backscatter coefficient from kidney parenchyma. A transverse isotropic correlation model is developed to explain how backscattered energy, which varies with the incident sound wave direction, is related to the anisotropic structure of the tissue. From the results we conclude that renal morphology scatters sound incoherently, and that complex mixtures of scattering structures of different sizes, number densities, and scattering strengths can be distinguished by analyzing backscatter in specific frequency channels—a spectroscopic approach. A $K$-space description of backscatter measurements from kidney cortex, including the effects of anisotopy, provides further support of our hypothesis regarding sources of acoustic scattering.

PACS numbers: 43.80.Cs, 43.80.Ev, 43.80.Jz

## INTRODUCTION

We are investigating nondestructive means of measuring important structural properties of biological tissue microanatomy using pulse-echo ultrasound. Our goal is to accurately describe the histology of live tissues. Through signal processing we seek to extract morphological information from the echo signals by comparing experimental echo-signal power spectra with analytically modeled spectra. The most straightforward approach to the forward problem of modeling the scattering process is to assume that tissues conduct sound as a fluid with spatially continuous, random, isotropic perturbations in elastic properties $\gamma(\mathbf{r})$ that scatter the sound weakly, elastically, and incoherently. If the random variable $\gamma(\mathbf{r})$ is highly correlated with the structure of interest, then one three-dimensional correlation function may be used to characterize the microstructure of the tissue, and the expressions that relate measured echo spectra to tissue morphology are known.[1–7] Such basic inverse methods have many applications, e.g., to characterize inhomogeneities in glass and polymers using scattering from laser light,[6] molecular bond lengths in liquids using neutron scattering,[7] solid-state structures using x-rays,[8] and to understand wave propagation in the atmosphere and ocean.[9,10]

Suprisingly, much information about the microstructure of biological tissues can be obtained with the very simple assumption that tissues are inhomogeneous fluids. For example, Mottley and Miller[11] and more recently Rose *et al.*[12] have developed models to describe how ultrasound is backscattered from structurally anisotropic heart muscle to explain why the echo intensity varies during the cardiac cycle. By understanding the anisotropic properties of the tissue, they were able to use measurements of backscattered intensity to diagnose abnormalities in the heart based on changes in myocardial microstructure.[13] Feleppa *et al.*[14] also used backscattered ultrasound to differentiate among different eye tumors; specifically, they measured quantities related to the average size and number density of scattering structures. With similar analytical methods, we found that the acoustic energy backscattered from a mixture of different size structures in the kidney could be discriminated using the echo spectrum,[15] and that it was possible to monitor changes in the size and number density of these structures that resulted from changes in renal function.[16] In each of the applications above, a more direct interpretation of backscattered ultrasound data was possible in terms of the tissue morphology once the scattering sites were identified.

As in muscle, the kidney has a random, anisotropic microstructure. An axis of symmetry is defined by the long axis of the nephron—the functional unit of the kidney. Nephrons are aligned, for the most part, radially from the center of the organ. Our analysis is focused on the cortical region of the kidney, the 1 cm-thick outer layer, because of its key role in renal function and pathology. We know from previous studies that the backscattered intensity from the renal cortex is greater when the axis of the incident sound beam is perpendicular to the long axis of the nephron than parallel.[15] For a fixed angle between the beam and tissue axes, we found that isotropic correlation coefficients accurately represented scattering sources in kidneys, i.e., scatterer size estimates were consistent with histological observations. This paper extends that analysis to include an anisotropic correlation model in the context of the forward problem. Successful implementation of this analysis could lead to a more general solution to the inverse problem and consequently a more reliable measure of kidney morphology.

## I. METHODS

### A. Scattering sources

Previous measurements in the 2–15-MHz frequency range have led us to conclude that the sources of acoustic scattering in the kidney are related to the nephron and associated blood vessels.[15,16] The elastic properties of basement

 0001-4966/95/97(1)/649/7/$6.00  

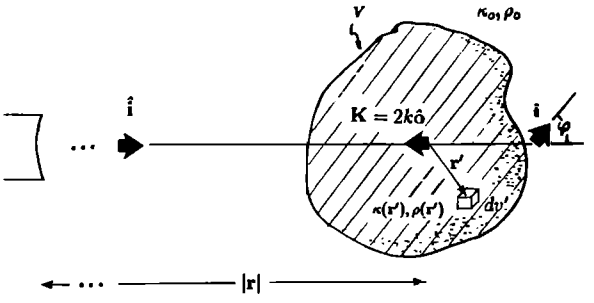


FIG. 1. An illustration of the general backscatter geometry.

membranes and smooth muscle vary sufficiently from the surrounding structures to assume that these are the specific scattering sites. Specifically, the measured value of Young's modulus for renal tubular basement membranes is $0.7–1.0\times10^9$ N/m$^2$ (Ref. 17)—on the order of that for pure tendon collagen: $5.1\times10^9$ N/m$^2$.[18] The evidence suggests that the physical properties of basement membranes surrounding small blood vessels are similar to those for tubules.[19] In fact, most of the structural rigidity of renal parenchyma can be attributed to the collagenous basement membranes that surround the components of nephrons and blood vessels.[17] Collagen has a Young's modulus at least three orders of magnitude greater than the surrounding tissues, e.g., the endothelium,[20] and a density 12% greater than that of water.[18] Among luminal components, basement membranes provide the largest fluctuation in elastic properties and hence the greatest opportunity to scatter sound. The situation is probably different at higher frequencies (>100 MHz); Kessler *et al.*[21] deduced that scattering from the collagenous intertubular regions is much greater than that from the nephron structures. However, at diagnostic frequencies, the basic functional units of the organ generate the most backscatter.

On a larger scale, the renal parenchyma is organized as a mixture of symmetric and asymmetric nephron-related structures that scatter sound. Renal tubules occupy most of the parenchymal volume. Convoluted parts of tubules are a closely packed tangle; along with the glomerulus these components are viewed in our model as randomly positioned, isotropic scattering structures. The ascending and descending loops, collecting tubules, and associated blood vessels are, for the most part, oriented along specific and known directions, and hence are viewed as anisotropic scattering structures. We show below that this simple conceptualization of renal morphology is sufficient to model acoustic interactions and explain why backscatter measurements in the kidney vary with the angle of the incident beam.

### B. Incoherent intensity formulation

Consider a unit-amplitude plane wave of sound $\exp(ik\hat{\mathbf{i}}\cdot\mathbf{r})$ that travels in the direction specified by the unit vector (bold face) $\hat{\mathbf{i}}$ and encounters a volume of renal tissue $V$ (Fig. 1). The position of the detector relative to $V$ is $\mathbf{r}$ and the wave number $k=2\pi/\lambda$ at wavelength $\lambda$. Ignoring thermal and viscous effects, the incident plane wave is scattered by fluctuations in the mass density $\rho(\mathbf{r}')$ and compressibility $\kappa(\mathbf{r}')$ of the medium.[22] The function $\gamma(\mathbf{r}')=f[\kappa(\mathbf{r}'),\rho(\mathbf{r}')]$ describes the spatial distribution of these fluctuations, which we refer to as the scattering structure. Note that the statistics of the echo signal depend on the *local* scattering structure. In pulse-echo measurements in the kidney, the structure in $V$, the volume of tissue occupied by the sound pulse at any instant of time, typically encompasses tens of nephrons. This is a standard physical model that we and others have used to investigate acoustic scattering in biological tissues. It has been described previously[23] and is summarized and applied below.

Assume that $\gamma(\mathbf{r})$ of the tissue is random, statistically homogeneous, and weakly scattering. Far from $V$, a detector intercepts an amount of scattered power given by the product of the incident intensity and a scattering cross section. We find the differential scattering cross section $\sigma$ by determining from pressure measurements the ensemble average of the differential power $\langle d\Pi\rangle$ scattered into the unit solid angle $d\Omega$ per incident intensity $I_i$:

$$\sigma(\mathbf{K})=\frac{\langle d\Pi(\mathbf{K})\rangle}{I_i d\Omega}$$
$$=\frac{k^4\langle\gamma^2\rangle V}{16\pi^2}\int\int\int_{-\infty}^{\infty} b_\gamma(\Delta\mathbf{r})e^{-i\mathbf{K}\cdot\Delta\mathbf{r}}dv_\Delta. \qquad (1)$$

Equation (1) is the usual single-scatter equation expressing the cross section as a function of the three-dimensional Fourier transform of the scattering structure.[22] The scattering vector $\mathbf{K}=k(\hat{\mathbf{o}}-\hat{\mathbf{i}})$ is the difference between wave numbers in the direction of the detector ($\hat{\mathbf{o}}$ for observer) and incident wave propagation $\hat{\mathbf{i}}$. For backscatter, $\mathbf{K}=2k\hat{\mathbf{o}}$. The difference vector $\Delta\mathbf{r}=\mathbf{r}_1'-\mathbf{r}_2'$ and $dv_\Delta=d\Delta\mathbf{r}$ (Fig. 1). Finally, the product of $\langle\gamma^2\rangle$, the mean-square fluctuation in medium properties, and $b_\gamma(\Delta\mathbf{r})$, the correlation coefficient for the medium, is the (auto)correlation function for the scattering medium. We are concerned with incoherent scattering only (since the coherent scattering component in tissue is small), so the correlation function entirely characterizes the scattering structure of the random medium.[23] In fact, the term "scatterer" is defined for media with continuous fluctuations in elastic properties by the correlation function. Tissues are considered as collections of scatterers of different size, shape, $\langle\gamma^2\rangle$, etc., that are spatially mixed, or in other words sums of $\gamma(\mathbf{r})$ functions, where each contributes to the net backscattered power in proportion to its volume fraction.

Analytically, the model involves plane waves interacting with an isolated volume $V$. Experimentally, however, an extended medium is probed and the volume responsible for scattering at any instant of time is determined by the resolution cell volume of the interrogating beam. In either case, we can eliminate the dependence of $\sigma$ on volume by dividing by $V$, and define the backscatter coefficient $\sigma_b$ as

$$\sigma_b(k,\varphi)=\frac{\sigma(2k\hat{\mathbf{o}})}{V}$$
$$=\frac{k^4\langle\gamma^2\rangle}{16\pi^2}\int\int\int_{-\infty}^{\infty} b_\gamma(\Delta\mathbf{r})e^{-i2k\hat{\mathbf{o}}\cdot\Delta\mathbf{r}}dv_\Delta, \qquad (2)$$

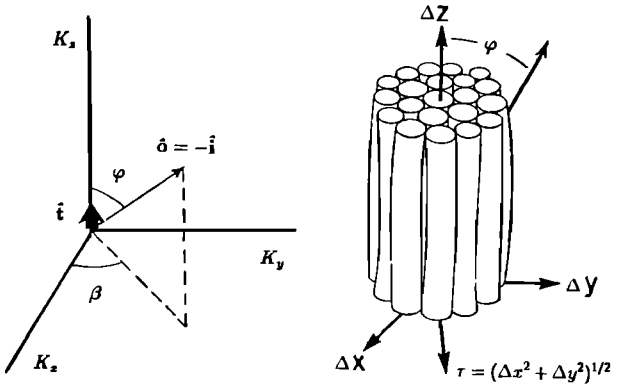


FIG. 2. Scattering geometry of the transverse isotropic correlation model. Spatial frequency (left) and spatial position (right) coordinates are illustrated. The unit vectors defining incident wave propagation $\hat{\mathbf{i}}$, direction of the detector $\hat{\mathbf{o}}$, and nephron orientation $\hat{\mathbf{t}}$ are specified. For backscatter, $\hat{\mathbf{o}} = -\hat{\mathbf{i}}$, and the angle between the interrogating beam and tissue structure is $\varphi = \cos^{-1}(\hat{\mathbf{o}} \cdot \hat{\mathbf{t}})$.

where $\varphi$ is the scanning angle discussed below. Equation (2) relates the backscattered power—a quantity we *measure*—to the correlation coefficient that characterizes the underlying microstructure—a function we *model* from histological observation.[15] In the forward problem, we input $b_\gamma$ into Eq. (2) to predict $\sigma_b$; in the inverse problem, we measure $\sigma_b$ and use Eq. (2) to estimate $b_\gamma$.

Backscatter coefficients are estimated from a few short-time echo waveform segments,[3] so the measurement uncertainty at specific frequencies can be large. To reduce uncertainty, we occasionally sum $\sigma_b$ values over a band of frequencies. The result is the integrated backscatter coefficient,

$$\mathrm{IBC}(\varphi) = \frac{1}{N_k} \sum_{i=1}^{N_k} \sigma_b(k_i, \varphi).$$

The spherical symmetry possible with isotropic structure allows simplification of the backscatter coefficient equation to a single integral:

$$\sigma_b(k) = \frac{k^3 \langle \gamma^2 \rangle}{8\pi} \int_0^\infty b_\gamma(\Delta r) \sin(2k\Delta r) \Delta r \, d\Delta r \quad \text{(isotropic)}. \tag{3}$$

Assuming the isotropic Gaussian form $b_\gamma(\Delta r) = \exp(-\Delta r^2/2d^2)$ and using Eq. (3), we were able to identify renal scattering structures in terms of their size (as related to the correlation length $d$) if we fixed the scanning angle between $\hat{\mathbf{o}}$ and the long axis of the nephron as defined by the unit vector $\hat{\mathbf{t}}$, i.e., $\varphi = \cos^{-1}(\hat{\mathbf{o}} \cdot \hat{\mathbf{t}})$ (Fig. 2).[15] To include the possibility of structural anisotropy in the model, we return to the more general treatment of Eq. (2), where $\sigma_b$ is expressed explicitly as a function of $k$ and $\varphi$.

### C. Correlation coefficients for renal tissues

Accurate descriptions of backscatter from anisotropic media using Eq. (2) must include spatial correlation coefficients that describe the three-dimensional structure of inhomogeneities encountered by a sound wave as it travels through the tissue. Levinson[24] suggested a *transverse isotropic* model to describe sound propagation in skeletal muscle. This model also describes renal cortical structure; it leads to a 3-D correlation coefficient that exhibits cylindrical symmetry and is isotropic in the $x$-$y$ plane. Aligning the axis of symmetry in the tissue and the $z$-axis, i.e., $\hat{\mathbf{t}} \cdot \hat{\mathbf{K}}_z = 1$, as illustrated in Fig. 2, then $b_\gamma(\Delta \mathbf{r}) = b_1(\Delta z) \times b_2(\Delta x, \Delta y)$ and Eq. (2) becomes the product of two transforms:[23]

$$\sigma_b(k,\varphi) = \frac{k^4 \langle \gamma^2 \rangle}{8\pi} \int_{-\infty}^{\infty} b_1(\Delta z) \; e^{-i2k\Delta z \cos\varphi} d\Delta z \times \int_0^\infty b_2(\tau) \; J_0(2k\tau \sin\varphi) \tau d\tau \quad \text{(transverse isotropic)}, \tag{4}$$

where $\tau = \sqrt{\Delta x^2 + \Delta y^2}$ and $J_0(\cdot)$ is a Bessel function of the first kind, zeroth order. The first integral is a Fourier transform of the correlation coefficient along the axis of symmetry and the second integral is a Hankel transform in the transverse plane.

Our previous experience at interpreting backscatter measurements in kidney tissues and our simplified view of renal histology suggest to us that renal tissues are a mixture of three types of structures: I, sparsely distributed, isotropic glomeruli; II, sparse, anisotropic blood vessels and tubule segments aligned along the $z$-axis; III, densely-packed, isotropic convoluted tubules. The correlation coefficients for these three structures are listed in Table I; each are based on a Gaussian function. (Note that $d_z$, $d_\tau$, and $d \equiv d_r$ are characteristic correlation lengths for the scattering continuum in the respective coordinates.) Substituting the isotropic models into Eq. (3) and the anisotropic models into Eq. (4) results in the analytic expressions for $\sigma_b$ listed in Table I for each scattering component.

### D. Discrete and continuous tissue models

Although the inhomogeneous continuum model of tissue structure has many advantages, it is often of interest to convert continuous quantities, such as the correlation length, into discrete quantities, such as the effective scatterer volume $V_s$ and diameter $D$. The scatterer volume has been defined previously as $V_s \equiv \int_{-\infty}^{\infty} b_\gamma(\Delta \mathbf{r}) dv_\Delta$.[23] For the three correlation coefficients proposed, it is straightforward to derive the effective scattering volumes listed in Table I. The effective size of such scatterers, $D$, is found by equating $V_s$ with the volume of a sphere.[3] Those results are also listed in Table I. Finally, we write $\langle \gamma^2 \rangle \simeq \bar{n} V_s \gamma_0^2$, where $\bar{n}$ is the mean number of scatterers per unit volume and $\gamma_0^2$ is the mean-square fluctuation in elastic properties *per scatterer*.

TABLE I. Correlation models and the corresponding backscatter coefficients and other features for three types of renal scattering structure: I=glomeruli (sparse, isotropic), II=blood vessels and tubule segments (sparse, transverse isotropic), and III=convoluted tubules (dense-packed, isotropic). The backscatter coefficient in the long-wavelength limit is $\sigma_0 = k^4 V_s \langle \gamma^2 \rangle / 16\pi^2$, $\tau = \sqrt{\Delta x^2 + \Delta y^2}$, $\varphi$ is the scanning angle, and the $d$'s are correlation lengths.

| | Correlation coefficient, $b_\gamma(\Delta \mathbf{r})$ (literature citations) | Backscatter coefficient, $\sigma_b$ | Scatterer volume, $V_s$ | Scatterer size, $D$ |
|---|---|---|---|---|
| I | $b_\gamma(\Delta r) = e^{-\Delta r^2/2d^2}$ (Ref. 9, p. 11; Ref. 22, p. 416; Ref. 30) | $\sigma_0 e^{-2k^2 d^2}$ | $(2\pi d^2)^{3/2}$ | $D = 2(3\sqrt{\pi/2})^{1/3} d \simeq 3.11d$ |
| II | $b_1(\Delta z) b_2(\tau) = e^{-\Delta z^2/2d_z^2} e^{-\tau^2/2d_\tau^2}$ (Ref. 23, p. 112) | $\sigma_0 e^{-2k^2(d_z^2 \cos^2\varphi + d_\tau^2 \sin^2\varphi)}$ | $(2\pi)^{3/2} d_z d_\tau^2$ | $D_z = \left(\frac{3\sqrt{2\pi}}{2}\right) d_z \simeq 3.76 d_z$<br>$D_\tau = 2\sqrt{2} d_\tau \simeq 2.83 d_\tau$ |
| III | $b_\gamma(\Delta r) = \left(1 - \frac{\Delta r^2}{3d^2}\right) e^{-\Delta r^2/2d^2}$ (Ref. 22, p. 439; Ref. 31) | $\sigma_0 \left[\sqrt{8\pi}\left(\frac{e}{3}\right)^{3/2} k^2 d^2\right] e^{-2k^2 d^2}$ | $\left(\frac{3}{e}\right)^{3/2} \frac{4\pi}{3} d^3$ | $D = 2\sqrt{\frac{3}{e}}\, d = 2.10d$ |

### E. Backscatter coefficient for renal tissues

The assumption of incoherent scattering enables us to express the backscatter coefficient for renal tissues as the sum of backscattered intensities from each structure. If $N_{\mathrm{I}}$, $N_{\mathrm{II}}$, and $N_{\mathrm{III}}$ are the numbers of structures of each type, then

$$\sigma_b(k,\varphi) = \sum_{\ell=1}^{N_{\mathrm{I}}} \sigma_b^{\mathrm{I}}(k)_\ell + \sum_{m=1}^{N_{\mathrm{II}}} \sigma_b^{\mathrm{II}}(k,\varphi)_m + \sum_{n=1}^{N_{\mathrm{III}}} \sigma_b^{\mathrm{III}}(k)_n, \quad (5)$$

and, from Table I,

$$\sigma_b(k,\varphi) = \frac{\pi k^4}{2} \left\{ \sum_{\ell=1}^{N_{\mathrm{I}}} [\tilde{n} d^6 \gamma_0^2]_\ell e^{-2k^2 d_\ell^2} + \sum_{m=1}^{N_{\mathrm{II}}} [\tilde{n} d_z^2 d_\tau^4 \gamma_0^2]_m e^{-2k^2(d_{zm}^2 \cos^2\varphi + d_{\tau m}^2 \sin^2\varphi)} + \sum_{n=1}^{N_{\mathrm{III}}} \left[\sqrt{8\pi}\left(\frac{e}{3}\right)^{3/2} \tilde{n} k^2 d^8 \gamma_0^2\right]_n e^{-2k^2 d_n^2} \right\}. \quad (6)$$

Equation (6) is a prediction of the backscatter from normal renal cortex that is based on the microscopic anatomy. From data in the anatomy and physiology literature on the average size and number of specific renal microstructures, predictions are made in the next section. Combining data from this literature and our previous measurements,[15,16] we now summarize in Table II the essential physical properties of renal cortex. The term "diameter" refers to an average cross-sectional diameter of the isotropic structures listed. For anisotropic structures, cross-sectional diameters are the smaller of the two values listed; the other is a coarse estimate of the lengths seen from light microscopy in the $y-z$ plane and are not the total lengths of those structures. Listed values for $\gamma_0^2$ are relative to that for the glomerulus. Each is a guess based on qualitative estimates of the amount of collagen in each structure. We used our previous estimate of $\gamma_{0,\mathrm{glom}}^2 = 0.001$.[15] Most of the data in Table II are rough estimates of highly variable biological quantities.

TABLE II. Properties of renal microanatomy.

| | Structure | Diameter ($\mu$m) | Number density ($\mathrm{mm}^{-3}$) | $\gamma_0^2/\gamma_{0,\mathrm{glom}}^2$ |
|---|---|---|---|---|
| Isotropic structures | glomerulus | 200 | 10 | 1.00 |
| | proximal convoluted tubule | 60 | 100 | 0.50 |
| | distal convoluted tubule | 40 | 100 | 0.50 |
| Anisotropic structures | descending loop | 15<br>500 | 10 | 0.25 |
| | ascending loop | 30<br>500 | 10 | 0.25 |
| | afferent arterioles | 50<br>100 | 50 | 2.0 |
| | efferent arterioles | 30<br>100 | 50 | 2.0 |
| | collecting tubules | 120<br>1000 | 0.1 | 2.0 |

## II. RESULTS

Combining the data in Table II with Eq. (6), we produced the values for $\sigma_b(k,\varphi)$ plotted as lines in Fig. 3. The abscissa is in units of temporal frequency $f = kc/2\pi$, where $c$ is the speed of sound. The scanning angle $\varphi = 0°$ indicates that the axis of the interrogating beam is parallel to the axis

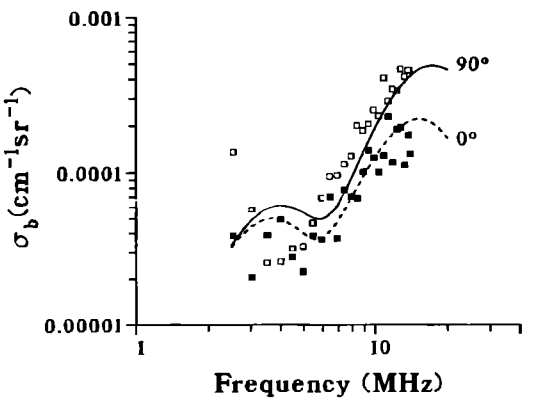


FIG. 3. Measured backscatter coefficient values (points) are compared with predicted values (curves) at two scanning angles, $\varphi = 0°$ (dashed line and closed points), and $\varphi = 90°$ (solid line and open points). Shown are data for a single sample of excised cortical tissue from a dog measured at 19 °C.

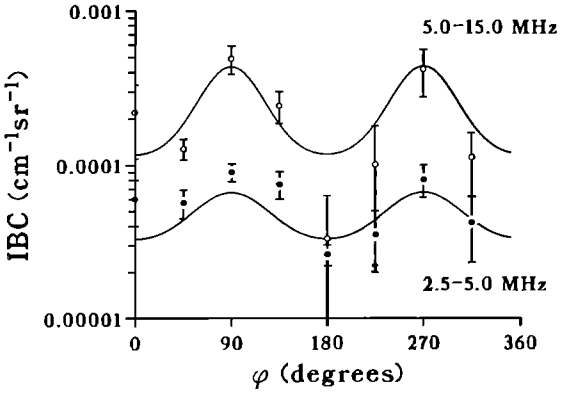


FIG. 4. Measured integrated backscatter coefficient values (points) and predicted values (lines) are plotted as a function of scanning angle for the high- and low-frequency bands indicated. Each data point indicates the average IBC value from four excised dog kidney samples measured at 19 °C. The error bars denote ±1 standard error.

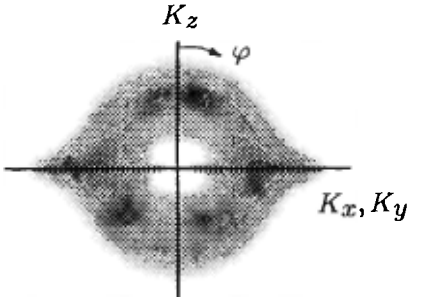


FIG. 5. The $K$-space diagram describes the distribution of backscatter coefficients for renal cortex as a function of spatial frequency, $k=|\mathbf{K}|$, and scanning angle, $\varphi$, that results from application of Eq. (6). The darkest areas indicate frequencies where backscatter is most intense. The axis of symmetry in tissue is aligned along the $z$ axis, and the horizontal axis is any line through the origin in the transverse $(x,y)$ plane of the tissue. For the anatomical structures listed in Table II, backscatter information is available up to temporal frequencies $f_{max}=ck_{max}/2\pi\simeq 30$ MHz. Adding smaller structures to the model, e.g., those at the cellular level, would increase $f_{max}$.

of the nephron, and $\varphi=90°$ indicates perpendicular incidence. Integrated backscatter coefficient (IBC) estimates for the frequency ranges indicated are plotted as a function of scanning angle in Fig. 4.

Predictions, as indicated by the curves in Figs. 3 and 4, are compared with measurement points reported earlier for kidney cortex.[15] All the data are for freshly excised normal dog kidneys; the data are from one tissue sample in Fig. 3 and an average of four tissue samples in Fig. 4. The curve representing perpendicular incidence in Fig. 3 was scaled to visually fit the data points. That one scale factor was then applied to all the curves in Figs. 3 and 4. The need for a scale factor reflects our lack of complete information regarding the elastic properties of microscopic renal anatomy. Nevertheless, the predictions do reflect the functional dependence of the measurements, particularly in the higher frequency range. The 5-MHz boundary between the two frequency ranges in Fig. 4 is based on our previous observations in the kidney: $\sigma_b$ properties are determined by ~200 $\mu$m-diam scatterers below this threshold and ~50$\mu$m-diam scatterers above this threshold.

The predicted values of $\sigma_b(k,\varphi)$ from Eq. (6) are also plotted in the polar $K$-space illustration of Fig. 5. The darkest areas indicate spatial frequencies for which the backscatter is most intense. The scanning angle $\varphi=0°$ is the $z$ axis, so that $\varphi=90°$ is the $x,y$-plane and perpendicular to the nephron axis. The dashed line in Fig. 3 is the same information provided by the $z$ axis in Fig. 5, as is the solid line in Fig. 3 and a radius in the $x,y$-plane in Fig. 5. Similarly, by averaging backscatter coefficients in Fig. 5 over frequency bands, we arrive at the curves in Fig. 4. The $K$-space description of backscatter is a convenient graphical method for examining results of the forward problem discussed in this paper as well as interpreting results of the inverse problem.[25–27]

## III. DISCUSSION

The overall agreement between the analytic model and the data in Figs. 3 and 4 indicates that Eq. (6) is a useful conceptual model for interpreting renal backscatter. Previously we found that $\sigma_b$ and IBC estimates varied significantly with $\varphi$, while scatterer size estimates (based on the frequency dependence of $\sigma_b$) did not.[15] Equation (6) provides one possible explanation. From Fig. 5 we see that renal backscatter is mostly isotropic except when the beam is nearly perpendicular to the nephon, at $\varphi\simeq 90°$ or 270°. The anisotropic components of the scattering structure produce a significant amount of backscatter only at near-perpendicular incidence. At other angles the backscatter cross section is so low that these structures effectively disappear. Consequently, changes in $\sigma_b$ as a function of $\varphi$ reflect changes in the number of contributing scatterers rather than the size of the structures. At frequencies less than 5 MHz, larger structures like the spherically shaped glomeruli produce the most backscatter, and therefore $\sigma_b$ is only weakly dependent on $\varphi$. At frequencies above 5 MHz, the smaller, anisotropic structures produce the most backscatter, generating more total backscatter at perdendicular incidence than at other angles.

Equation (6) can be extended to include greater diversity in scatterer size than that outlined in Table II. For example, our histological studies of the kidney[15] show that the glomerular diameter is approximately normally distributed about a mean value. This added diversity may be included in the model simply by convolving each of the $\sigma_b$ terms on the right-hand side of Eq. (5) with a function $\mathcal{J}(d)$ that describes the number of scatterers in the distribution about the mean correlation length $d$. That is,

$$\sigma_{b'}^{1}(k,d)_{\mathcal{J}}=\frac{1}{\bar{n}}\sum_{d'}\sigma_b^{1}(k,d')_{\mathcal{J}}\,\mathcal{J}(d-d').$$

For $\mathcal{J}=\bar{n}\delta(d-d')$, we return to the result of Eq. (6). However, using $\mathcal{J}=\text{Gaussian}(d,s^2)$, we found that the increased size diversity, i.e., larger values of $s^2$, tended to flatten the curves for $\sigma_b(k)$ in Fig. 3 for all $\varphi$, in conflict with measurements. Adding size diversity did not improve the agreement between predicted and measured values and therefore was not used in Figs. 3–5.

It is interesting to contrast observations of acoustic backscatter in the kidney with that in the heart. As in the

kidney, myocardial backscatter is maximum when sound waves travel perdendicular to the aligned structure (muscle fibers) and minimum along the structure.[11] Therefore, a large part of the variation in backscatter with cardiac cycle can be attributed to a changing alignment between muscle fibers and the sound beam as the heart contracts and relaxes. However, Wear *et al.*[28] have shown that there is also a small but significant change in the frequency dependence of backscatter during the cardiac cycle that may be attributed to changes in the effective scatterer size. They found that isotonic contractions distort the shape of the myocytes so that their cross-sectional diameters vary during the cardiac cycle.[32] Backscattered ultrasound can also be used in the live kidney to detect changes in the size of renal structures altered by physiological manipulation[16] or disease.[29]

In our model, collagenous basement membranes act as scattering sources. Similarly, in the myocardial model of backscatter proposed by Rose *et al.*,[12] the scattering sources are assumed to be the extracellular collagen surrounding the myocytes. One obvious difference between the heart and kidney backscatter models is that Rose represents myocardial scatterers as an ensemble of discrete prolate spheroids, while we represent renal scatterers by a Gaussian correlation function. There is little difference among the predictions for discrete and continuous models when the scatterer size is on the order of the wavelength or less, i.e., $D/\lambda \leq 1$. At shorter wavelengths, discrete scatterers display sharp spectral minima (resonances) and the Gaussian correlation coefficient vanishes; neither of these effects have been seen in tissue measurements. In the size-frequency range where $D/\lambda \leq 1$, discrete and continuous formulations provide equivalent predictive accuracy—one may offer more mathematical convenience or greater physical intuition, but both are representative of measurements in tissue. Further development of backscatter models depends much more on improving our understanding of the physical properties of tissue microstructure.

Note that a dense-packed correlation model was used to describe scattering from convoluted tubules. This was necessary to match the model to the data in Fig. 3 at frequencies above 5 MHz. The backscatter coefficient from dense-packed scatterers has a greater frequency dependence ($f^6$) than that predicted for Rayleigh scattering ($f^4$). Convoluted tubules appear histologically as a dense tangle of tubules that occupy most of the cortical volume, suggesting that the dense-packed, isotropic Gaussian correlation model is reasonable. It is also possible that structures smaller than those considered in Table II, which contribute significantly to backscatter at frequencies above 10 MHz, might be needed to complete the model. We have omitted smaller structures in the analysis, on the order of the cell size, because there is little or no detailed data on their elastic properties.

Equation (6) is intended to be descriptive of renal backscatter in the diagnostic range of frequencies: 2–15 MHz. In that range, it is possible to study changes in glomerular structure for live organs by analyzing backscatter between 2 and 5 MHz. Information about properties of arterioles and tubules may be obtained from backscatter coefficients at frequencies between 5 and 15 MHz.[16]

## IV. CONCLUSIONS

This study extends our previous ultrasonic analysis of renal microanatomy to three dimensions by including a directionally dependent correlation function to represent scattering sites in tissue. The intensity backscattered from normal renal parenchyma between 2 and 15 MHz is consistent with an incoherent summation of sound waves scattered from tissue structures on the scale of the nephron and associated blood vessels. Most variation in the backscatter coefficient with scanning angle appears to be caused by changes in the number of structures per volume of tissue that scatter sound.

## ACKNOWLEDGMENTS

The author gratefully acknowledges the essential contributions of Tim Hall, John Wood, and Larry Cook. This work was supported by NIH Grant No. DK43007 and the Clinical Radiology Foundation at KUMC.

[1] J.A. Campbell and R.C. Waag, "Normalization of ultrasonic scattering measurements to obtain average differential scattering cross sections for tissues," J. Acoust. Soc. Am. **74**, 393–399 (1983).
[2] F.L. Lizzi, M. Greenebaum, E.J. Feleppa, M. Elbaum, and D.J. Coleman, "Theoretical framework for spectrum analysis in ultrasonic tissue characterization," J. Acoust. Soc. Am. **73**, 1366–1373 (1983).
[3] M.F. Insana, R.F. Wagner, D.G. Brown, and T.J. Hall, "Describing small-scale structure in random media using pulse-echo ultrasound," J. Acoust. Soc. Am. **87**, 179–192 (1990).
[4] R.C. Chivers, "The scattering of ultrasound by human tissues—some theoretical models," Ultrasound Med. Biol. **3**, 1–13 (1977).
[5] J.C. Gore and S. Leeman, "Ultrasonic backscattering from human tissues: a realistic model," Phys. Med. Biol. **22**, 317–326 (1977).
[6] Y. Miyazaki, "Light scattering of laser beams by random micro-inhomogeneities in glasses and polymers," Japanese J. Appl. Phys. **13**, 1238–1248 (1974).
[7] P.A. Egelstaff, C.G. Gray, K.E. Gubbins, and K.C. Mo, "Theory of inelastic neutron scattering from molecular fluids," J. Stat. Phys. **13**, 315–330 (1975).
[8] M. Tobiyama, I. Endo, T. Monaka *et al.*, "Determination of atomic form factors by means of coherent bremsstrahlung," Phys. Rev. B **44**, 9248–9258 (1991).
[9] L.A. Chernov, *Wave Propagation in a Random Medium* (McGraw–Hill, New York, 1960).
[10] V.I. Tatarski, *Wave Propagation in a Turbulent Medium* (McGraw–Hill, New York, 1961).
[11] J.G. Mottley and J.G. Miller, "Anisotropy of the ultrasonic backscatter of myocardial tissue: I. Theory and measurement *in vitro*," J. Acoust. Soc. Am. **83**, 755–761 (1988).
[12] J.H. Rose, M.R. Kaufmann, S.A. Wickline, C.S. Hall, and J.G. Miller, "A proposed microscopic elastic wave theory for ultrasonic backscatter from myocardial tissue," J. Acoust. Soc. Am. (submitted 1994).
[13] Z. Vered, B. Barzilai, G.A. Mohr, L. J. Thomas III, R. Genton, B. E. Sobel, T. A. Shoup, H. E. Melton, J. G. Miller, and J. E. Perez, "Quantitative ultrasonic tissue characterization with real-time integrated backscatter imaging in normal human subjects and in patients with dilated cardiomyopathy," Circulation **76**, 1067–1073 (1987).
[14] E.J. Feleppa, F.L. Lizzi, D.J. Coleman, and M.M. Yaremko, "Diagnostic spectrum analysis in ophthalmology: a physical perspective," Ultrasound Med. Biol. **12**, 623–631 (1986).
[15] M.F. Insana, T.J. Hall, and J.L. Fishback, "Identifying acoustic scattering sources in normal renal parenchyma from the anisotropy in acoustic properties," Ultrasound Med. Biol. **17**, 613–626 (1991).
[16] M.F. Insana, J.G. Wood, and T.J. Hall, "Identifying acoustic scattering sources in normal renal parenchyma *in vivo* by varying arterial and ureteral pressures," Ultrasound Med. Biol. **18**, 587–599 (1992).
[17] L.W. Welling and J.J. Grantham, "Physical properties of isolated perfused renal tubules and tubular basement membranes," J. Clin. Invest. **51**, 1063–1075 (1972).

[18]S. Cusack and A. Miller, "Determination of the elastic constants of collagen by Brillouin light scattering," J. Mol. Biol. **135**, 39–51 (1979).
[19]M.E. Murphy and P.C. Johnson, "Possible contribution of basement membrane to the structural rigidity of blood capillaries," Microvascular Res. **9**, 242–245 (1975).
[20]S. Fields and F. Dunn, "Correlation of echographic visualizability of tissue with biological composition and physiological state," J. Acoust. Soc. Am. **54**, 809–812 (1973).
[21]L.W. Kessler, S.I. Fields, and F. Dunn, "Acoustic microscopy of mammalian kidney," J. Clin. Ultrasound **2**, 317–320 (1975).
[22]P.M. Morse and K.U. Ingard, *Theoretical Acoustics* (McGraw–Hill, New York, 1968), Chaps. 7 and 8.
[23]M.F. Insana and D.G. Brown, "Acoustic scattering theory applied to soft biological tissues," in *Ultrasonic Scattering in Biological Tissues*, edited by K.K. Shung and G.A. Thieme (CRC, Boca Raton, 1993), pp. 75–124.
[24]S.F. Levinson, "Ultrasound propagation in anisotropic soft tissues: the application of linear elastic theory," J. Biomech. **20**, 251–260 (1987).
[25]J.F. Greenleaf, "A graphical description of scattering," Ultrasound Med. Biol. **12**, 603–609 (1986).
[26]R.M. Lerner and R.C. Waag, "Wave space interpretation of scattered ultrasound," Ultrasound Med. Biol. **14**, 97–102 (1988).
[27]R.C. Waag and J.P. Astheimer, "Measurement system effects in ultrasonic scattering experiments," in *Ultrasonic Scattering in Biological Tissues*, edited by K.K. Shung and G.A. Thieme (CRC, Boca Raton, 1993).
[28]K.A. Wear, M.R. Milunski, S.A. Wickline, J.E. Perez, B.E. Sobel, and J.G. Miller, "Contraction-related variation in frequency dependence of acoustic properties of canine myocardium," J. Acoust. Soc. Am. **86**, 2067–2072 (1989).
[29]B.S. Garra, M.F. Insana, I.A. Sesterhenn, T.J. Hall, R.F. Wagner, C. Rotellar, J. Winchester, and R.K. Zeman, "Quantitative ultrasonic detection of parenchymal structural change in diffuse renal disease," Invest. Radiol. **29**, 134–140 (1994).
[30]F.L. Lizzi, M. Ostromogilsky, E.J. Feleppa, M.C. Rorke, and M.M. Yaremko, "Relationship of ultrasonic spectral parameters to features of tissue microstructure," IEEE Trans. Ultrason. Ferroelectr. Freq. Control **UFFC-34**, 319–329 (1987).
[31]J.A. Campbell and R.C. Waag, "Ultrasonic scattering properties of three random media with implications for tissue characterization," J. Acoust. Soc. Am. **75**, 1879–1886 (1984).
[32]K.A. Wear, T.A. Shoup, and R.L. Popp, "Ultrasonic characterization of canine myocardial contraction," IEEE Trans. Ultrason. Ferroelectr. Freq. Control **UFFC-33**, 347–353 (1986).